

Stellar Outflows Driven by Magnetized Wide-Angle Winds

T. A. Gardiner¹, A. Frank¹ and L. Hartmann²

¹ *Dept. of Physics and Astronomy,
University of Rochester, Rochester, NY 14627-0171*

² *Harvard-Smithsonian Center for Astrophysics,
Cambridge, MA 02138*

ABSTRACT

We present two-dimensional, cylindrically symmetric simulations of hydrodynamic and magnetohydrodynamic (MHD) wide-angle winds interacting with a collapsing environment. These simulations have direct relevance to young stellar objects (YSOs). The results may also be of use in the study of collimated outflows from proto-planetary and planetary nebulae. We study a range of wind configurations consistent with asymptotic MHD wind collimation. The degree of collimation is parameterized by the ratio of the wind density at the pole to that of the equator. We find that a toroidal magnetic field can have a significant influence on the resulting outflow, giving rise to a very dense, jet-like flow in the post-shock region. The properties of the flow in this region are similar to the asymptotic state of a collimated MHD wind. We conclude that wide-angle MHD winds are quite likely capable of driving molecular outflows. Due to difficulty in treating MHD winds ab-initio in simulations we choose magnetic field strengths in the wind consistent slow magnetic rotators. While MHD launched winds will be in the fast rotator regime we discuss how our results, which rely on toroidal pinch effects, will hold for stronger field strengths.

Subject headings: ISM: jets and outflows — stars: winds, outflows — magnetic fields — magnetohydrodynamics: MHD

1. INTRODUCTION

Newly formed stars drive copious mass back into the environments which gave them birth. Stars at the end of their lives also drive strong outflows into the interstellar medium.

Mass loss from young stellar objects (YSOs) takes the form of highly collimated Herbig-Haro jets and molecular outflows (Reipurth 1997), while in low mass, evolved stars, mass loss takes the form of proto-planetary (PPNe) and planetary nebulae (PNe) (Balick 2000). High resolution observations of PPNe and PNe have revealed outflow features that are very similar to those found in YSOs (Sahai 2000). In particular, recent visible and molecular observations of PPNe and young PNe have revealed the presence of both well collimated jets and broader wind-swept bubbles. Even though PNe and YSOs are at different extremes of stellar evolution, the similarity manifested in their mass loss raises intriguing questions about the processes driving and shaping their outflows. For example, outflows from PPNe appear to have more momentum than can be supplied by the central star’s luminosity ($L_*/c \ll \dot{M}V$) (Alcolea *et al.* 2000), a situation which also occurs in YSOs. Recently, it has been shown that PPNe winds may derive their acceleration and collimation from the same magneto-hydrodynamic (MHD) forces believed to be at work in YSOs (Blackman, Frank & Welch 2001). Thus, there exists the possibility that a cross fertilization between the two fields may yield some insights into the origins of magnetized winds and their dynamical interaction with surrounding media. In this paper we focus on one specific issue in the study of stellar outflows: the role of shocked magnetic fields in shaping wind blown bubbles.

Wind blown bubbles have long been part of the theoretical explanation for PNe. The interaction of a fast wind from the hot central star of a PN with a slower, denser, and possibly aspherical AGB wind has been successful at explaining many properties of spherical PN (Kwok *et al.* 1978; Kahn & West 1985; Balick 1987; Icke 1988; Frank *et al.* 1993; Mellema 1997). New images of PPNe and young PNe, however, show features which can not be explained with a purely hydrodynamic interacting stellar wind model (Delamarter *et al.* 2000). With an eye toward understanding the intermediate to large scale shaping of PNe, Chevalier & Luo (1994) drew attention to the role of shock amplified toroidal magnetic fields in the wind-blown bubble scenario. We will refer to this as the magnetized wind-blown bubble (MWBB) model. A number of MWBB studies (Różycka & Franco 1996; García-Segura 1997; García-Segura *et al.* 1999) have demonstrated the model’s ability to create a rich variety of structures in the shocked regions of the flow. A central assumption of the MWBB model, however, is that the magnetic field strength in the central wind is sufficiently weak that intrinsic MHD collimation can be ignored. Gardiner & Frank (2001) recently studied the role of intrinsic collimation in the magnetized central wind showing that for many cases of interest, the freely expanding wind may experience significant collimation before it passes through the wind shock. In this paper we borrow the central idea from Chevalier & Luo (1994) regarding the shock amplification of toroidal magnetic fields and use the results of Gardiner & Frank (2001) to explore MHD, wide-angle wind driven outflows from YSOs.

Wind blown bubbles have also been invoked to explain YSO outflows. Shu *et al.* (1991) presented a model wherein a radially directed wind from a central source sweeps up strongly cooling ambient material like a snowplow. This *snowplow* model was critically examined by Masson & Chernin (1992) who noted that without extreme choices for the angular variation of ambient density and wind momentum it is difficult to match the observed mass versus velocity relation. They concluded that the driving force was unlikely to originate from a wide angle wind, but rather from a collimated, and possibly precessing, jet (Chernin & Masson 1995). Li & Shu (1996b), however, found that taking the wind parameters from X-wind model (Shu *et al.* 1995) and the ambient density as described by Li & Shu (1996b) an improved agreement with observations could be found. More recently, Matzner & McKee (1999) have argued that the asymptotic form of the density and toroidal magnetic field strength in the X-wind model (Shu *et al.* 1995) is generally applicable to all MHD outflows. Moreover they argue that the power-law mass vs. velocity relations typically observed for molecular outflows is recovered for a wide variety of ambient density distributions.

More recently, Delamarter *et al.* (2000) used time-dependent, purely hydrodynamic simulations of winds driven into infalling environments, characteristic of YSOs (Hartman *et al.* 1996), to study very young outflows (Wilkin & Stahler 1998). It was concluded that the snowplow model could not embrace nonlinear effects which may yield changes in momentum distributions in the resultant outflows. Delamarter *et al.* (2000) focused on the effect of shock-focusing, where the wind strikes the bubble shell obliquely and is redirected to flow along the walls of the shell. The flow of shocked wind material toward the poles has the effect of substantially changing the bubble’s morphology and evolution from that obtained in a simple snowplow model. *In addition, it was found that inflow ram pressure produced significant collimation.* In a different set of purely hydrodynamic simulations, Lee *et al.* (2001) examine both wind driven and jet driven models, concluding that only some observed outflows have properties consistent with wide-angle winds. Their wind blown bubble simulations do not, however, include infall and their use of an isothermal equation of state produces what appear to be very thin bubble shells. It is not clear if shock-focusing could become manifest in such conditions. Thus, even in pure hydrodynamic models the applicability of wind blown models remains an open issue.

Magnetic forces are expected to play a central role in launching and collimating YSO (and perhaps PPN) winds. Steady state models of MHD winds have been quite successful at articulating their characteristic distributions of mass and momentum (Shu *et al.* 1995; Pudritz & Konigl 2000). These models rely on a detailed solution of cross-field force balance via the Grad-Shafranov equation (Shu *et al.* 1991). Interaction with an ambient medium will alter these distribution as the wind passes through the shock bounding the inner edge of the outflow shell. The subsequent redistribution of mass, momentum, and magnetic

energy, as the plasma seeks equilibrium, will alter downstream (post-shock) regions of the flow from what might be expected via steady MHD wind models. If the sources are variable, substantial portions of the outflow cavities may behave differently as well. Thus the time-dependent interaction of MHD winds with their environments is a rich subject with important consequences for both YSOs and PNe.

In this paper we describe a set of calculations aimed at elucidating the interaction of MHD winds from a central source with a collapsing environment applicable to YSOs. We show that magnetized wide-angle winds differ significantly from their hydrodynamic counterparts and offer a viable explanation for molecular outflows even for slow magnetic rotators. This paper focuses only on the flow pattern achieved in the simulations. In a second paper we plan to discuss observational consequences of MHD wind driven outflows. We also note that due to the difficulty in treating magneto-centrifugally driven winds *ab-initio* in larger-scale simulations we choose magnetic field strengths in the wind consistent with slow magnetic rotators. While MHD launched winds will be in the fast rotator regime our results, relying on toroidal pinch effects, will hold for stronger field strengths. This level of abstraction allows us to isolate key effects in the evolution of magnetized winds which will result regardless of the field strengths and builds on previous studies which only considered pure hydrodynamic winds (Delamarter *et al.* 2000; Lee *et al.* 2001).

2. SIMULATION DETAILS

We present axisymmetric (2.5-D) numerical simulations calculated with a recently constructed Godunov type scheme for the system of ideal MHD. We implement the “Positive Scheme” (Liu & Lax 1996; Lax & Liu 1998) which makes use of a Roe linearized Jacobian matrix, *e.g.* Cargo & Gallice (1997). Optically thin radiative cooling is included by making use of the Dalgarno-McCray coronal cooling curve in tabulated form. Below 10^4 K the cooling is turned off. The cooling is implicitly differenced and solved using Brent’s algorithm (Numerical Recipes). The gravitational field of a central source is included using a first order, explicit Euler step. The cooling and gravitational terms are operator split from the MHD integration. The system of ideal MHD is integrated in an unsplit (directional splitting) fashion and second order accuracy is obtained through the Runge-Kutta method of Shu & Osher (1989).

The simulations presented in this paper use the $f' = 10$ simulation of Delamarter *et al.* (2000) as a starting point. The parameter

$$f' = \frac{\dot{M}_i}{\dot{M}_w}, \quad (1)$$

measures the ratio of the inflow mass flux to the wind mass flux. (Note that Table 1 in that paper contains typographical errors such that the infall mass flux should read \dot{M}_i and be in units of $10^{-7} M_\odot \text{ yr}^{-1}$ rather than $10^{-6} M_\odot \text{ yr}^{-1}$.) The environment is derived from simulations of a collapsing, rotating, axially symmetric sheet (Hartman *et al.* 1996). This study is extended in two ways. First, a magnetic field, which is believed to be the principal agent for wind launching and collimation, is introduced into the wind. Second, an angular variation of the wind density and magnetic field strength is introduced which is consistent with magnetic collimation at small radii.

It is straight-forward to show from the ϕ -component of the induction equation and the momentum equation that for $r \gg R_A$, where r is the spherical radius and R_A is the Alfvén radius,

$$\frac{B_\phi}{B_r} \approx \frac{-r\Omega \sin(\theta)}{v_r}.$$

The other parameters in this equation are Ω , the angular velocity at the base of the wind, and v_r , the radial wind velocity. This expression assumes a radially directed wind and solid body rotation. From the expression above we find that the toroidal field will likely dominate over the poloidal. Thus for $\sin(\theta) = 1/\sqrt{2}$, $v_r = 200 \text{ km s}^{-1}$, $r = 13 \text{ AU}$ we find $B_\phi/B_r \sim 6 \times 10^6 * \Omega$ where $\Omega = 2\pi/\tau$ and τ is the rotational period in seconds. It is not immediately clear which rotational period should be used in these expressions, the stellar rotational period, or the period of the gas in orbit around the YSO at a few stellar radii. For example, using the sun’s rotational period of 25 days we find $B_\phi/B_r \sim 20$. The higher rotation rates associated with YSOs should lead to stronger field ratios than calculated above and it is likely that $B_\phi/B_r > 100$. Moreover, in the presence of cooling the post-shock toroidal field strength can be amplified by orders of magnitude over its pre-shock value. Thus we begin our calculations by approximating the magnetic field in the wind as being purely toroidal. The strength of the toroidal magnetic field is controlled by the parameter $\sigma = (V_m/V_\infty)^3$ where V_m is the Michel velocity and V_∞ is the asymptotic wind velocity (Michel 1969; Belcher & MacGregor 1976; Gardiner & Frank 2001). In this study we will be primarily concerned with slow magnetic rotators, *i.e.* $\sigma \ll 1$. As we will see, since the magnetic field will come to strongly influence the evolution of the outflow, our results will be valid for fast rotators (and their stronger initial fields) as well.

The angular variation of the wind density and magnetic field is parameterized by χ , the ratio of the density at the pole ($\theta = 0$) to the density at the equator ($\theta = \pi/2$) in the wind. We refer to this ratio as the pole to equator density contrast and study the range of $1 \leq \chi \leq 9$. Given these two parameters, σ and χ , the wind density

$$\rho(r, \theta) = \left(\frac{\dot{M}}{4\pi r^2 V_\infty} \right) \left(\frac{\sqrt{\chi}}{\chi \sin^2(\theta) + \cos^2(\theta)} \right), \quad (2)$$

and toroidal magnetic field component

$$B_\phi(r, \theta) = \left(\frac{\sqrt{\sigma \dot{M} V_\infty} \sin(\theta)}{r} \right) \left(\frac{\sqrt{\chi}}{\chi \sin^2(\theta) + \cos^2(\theta)} \right). \quad (3)$$

In these expressions we’ve assumed that r is sufficiently large that the radial component of the wind velocity $v_r \approx V_\infty$. For $\chi = 1$ we obtain the classic split monopole, spherically symmetric wind conditions. For $(\chi - 1) \sin^2(\theta) \gg 1$ the density and toroidal field strength take the form $B_\phi \propto 1/\varpi$ and $\rho \propto 1/\varpi^2$, where $\varpi = r \sin(\theta)$. This form is consistent with the asymptotic form of the X-wind solution (Shu *et al.* 1995) and in this way the parameter χ models the intrinsic magnetic collimation at small radii. The parameters χ and σ are not actually independent of one another, but rather are connected through a self consistent solution at small radii, *i.e.* the launching and collimation process. However, since a complete simulation of the wind launching, collimation, and propagation is beyond the scope of this paper, we will treat them as weakly independent.

A few details remain to complete the specification of the wind. All simulations use a wind with temperature 10^4 K. The wind mass loss rate is $10^{-7} M_\odot \text{ yr}^{-1}$ and the velocity is taken to be 200 km s^{-1} . The “wind-sphere” (the boundary on which the wind conditions are set) has a radius of 11.25 AU or 30 grid cells. The toroidal magnetic field strength as shown above gives rise to a current sheet at the equator ($\theta = \pi/2$). To smooth out this singularity, we impose a linear variation on the toroidal magnetic field within 6 degrees of the equator. At the radius of the wind-sphere this affects approximately 3 grid cells adjacent to the equatorial plane. This should not influence the results of the simulations. Finally, note that

$$\frac{2}{\pi} \int_0^{\pi/2} \frac{\sqrt{\chi}}{\chi \sin^2(\theta) + \cos^2(\theta)} d\theta = 1. \quad (4)$$

Hence the mass loss rate is independent of the parameter χ .

3. RESULTS

Here we focus on the effect of magnetic fields in shaping wide-angle wind blown bubbles by showing the results of five simulations where the field strength (σ) and density stratification (χ) vary. In figures 1 through 4 we present the logarithm of density for the four combinations of $\sigma = 0, 0.01$ and $\chi = 1, 9$. Figure 5 shows a time sequence of logarithmic density maps for a more highly stratified model ($\sigma = 0.01, \chi = 100$). Note that $\sigma = 0.01$ is approximately equal to the value for the solar wind, for which $\sigma \approx 0.009$, indicating that this is a slow magnetic rotator, *i.e.* the magnetic field is relatively unimportant in accelerating the wind. As we shall see, however, this does not imply that the field is dynamically

unimportant with respect to shaping the bubble (Chevalier & Luo 1994; García-Segura *et al.* 1999). We note also that our simulations are relevant to the earliest phase of dynamical shaping since the length and time scales are relatively short ($L < 10^{16}$ cm, $t < 50$ y). Our explicit goal is to understand the role of shock amplified magnetic fields and wide-angle winds in shaping the early evolution of the outflow.

First consider the hydrodynamic models shown in Figure 1 and 2 ($\sigma = 0$, $\chi = 1, 9$). In the spherical wind ($\chi = 1$) case the outflow assumes a characteristic bipolar morphology. As Wilkin & Stahler (1998) and Delamarter *et al.* (2000) have shown, the aspherical nature of the outflow is the result of both inertial and infall ram pressure gradients. The morphology is also effected by the development of shock focusing where the freely flowing wind impinges the wind shock at an oblique angle. This leaves high velocity (potentially supersonic) post-shock gas flowing tangential to the shock along the walls of the bubble shell. This post-shock material flows toward the bubble’s axis altering its shape and momentum distribution (Cantó *et al.* 1988; Giuliani 1982). Simplified calculations by Delamarter *et al.* (2000) show that mixing of the shocked ambient and shocked wind material cannot a priori, be expected to quench shock focusing. In addition Delamarter *et al.* (2000) found that the time-scale for mixing was comparable to the outflow evolution time-scale meaning the bubble shell was unlikely to be fully mixed. Thus the shape of the outflow may deviate from what is predicted by simple snowplow models.

In Figure 2 we see the effect of the angular variation in the wind ram pressure (density stratification in a wide-angle wind, $\chi = 9$). As has been shown for nebulae surrounding Luminous Blue Variables, aspherical winds flowing into spherical environments can produce bipolar bubbles when cooling in the shell is effective (Frank *et al.* 1998). The higher wind ram pressure at the poles increases the shock speed at the tip of the bubble, elongating the outflow. This in turn has a secondary effect of increasing the obliquity of the wind shock relative to the freely expanding wind. The degree of shock focusing is thereby increased creating a converging conical flow at the symmetry axis. Converging conical flows can be quite effective at producing well collimated jets from the tips of wind blown bubbles. This effect has been studied in analytical models (Cantó *et al.* 1988), numerical simulations (Mellema & Frank 1997), and more recently, laboratory experiments (Lebedev *et al.* 2002) which have shown the stability of the collimation process.

In figures 3 and 4 we present the logarithm of density for magnetohydrodynamic wind calculations with $\sigma = 0.01$ and $\chi = 1, 9$. Compared with the hydrodynamic calculations, the magnetic field in the wind has modified the outflow evolution considerably. In both of these figures we find a dense, jet-like flow aligned with the symmetry axis. These features have been documented before in spherical wind models appropriate to PPNe (García-Segura

et al. 1999). In our simulations we are able to investigate a new phenomenon, the effect of wind stratification on the subsequent MWBB evolution.

The origin of axial feature is a simple result of shock amplified toroidal magnetic fields. The magnetic field is amplified after it passes through the wind shock. Strong cooling further compresses the field, decreasing $\beta = 8\pi P_{gas}/B^2$ and leaving the Lorentz force out of balance with gas pressure gradients. When the magnetosonic wave speed is comparable to or greater than the radial expansion velocity of the bubble, the plasma in the post-shock region will be approximately in force balance. If the radiative cooling decreases β to less than or equal to 1, the Lorentz force will drive the plasma toward the axis. Gas pressure near the axis grows due to the compression driven by the magnetic pinch. While a new radial force balance will eventually be established, as we discuss below, the gas and magnetic pressures lead to expansion parallel and anti-parallel to the z -axis. The jets expand along the z -axis leading to an acceleration of the “head” of the bubble. When the wind is spherical, the jet can also push back toward the star creating a dense “spike” that changes the wind shock geometry from convex to concave. The development of such backflowing jets has been seen in previous studies (Różycka & Franco 1996; García-Segura *et al.* 1999).

A new feature observed in our simulations is shown in Figure 4 where density stratification in a wide-angle wind produces increased ram pressure near the axis. The ram pressure gradient and corresponding shock focused flow inhibits the backflowing jet. Thus, for χ sufficiently large, a density stratified, wide-angle wind produces a convex wind shock rather than the concave feature seen in Figure 3. The quenching of the backflow implies the jets will not appear to extend back to the source, and one expects hollow cavities with jets appearing some distance above the source inside the outflow.

Figure 5 shows a time sequence for a highly stratified wind, $\sigma = 0.01$ and $\chi = 100$. In this model the flow is highly elongated and is quite similar in appearance to simulations of toroidally dominated MHD jets (Cerqueira & de Gouveia Dal Pino 2001; Frank *et al.* 1998, 2000; Stone & Hardee 2000; O’Sullivan & Ray 2000). The long term evolution results in a highly cylindrically stratified, jet-like outflow. Note that near the base of the flow the divergent streamlines are still able to carve out a hollow cavity.

The formation of a steady, dense, well-collimated jet downstream of the wind shock (as is seen in figures 3, 4 and 5) requires the establishment of a new MHD equilibria. A more detailed consideration of the simulation results along with simple results from magneto-statics shows how this occurs (Choudhuri 1998). Establishment of a force balance in a cylindrical plasma column requires

$$\frac{dp_g}{d\varpi} - \frac{\rho v_\phi^2}{\varpi} = -\frac{1}{\varpi^2} \frac{d}{d\varpi} \frac{\varpi^2 B_\phi^2}{8\pi} \quad (5)$$

where the term on the right hand side can be decomposed in to magnetic pressure and tension components ($\frac{d}{d\varpi} \frac{B_\phi^2}{8\pi} + \frac{B_\phi^2}{4\pi\varpi}$). If the rotation in the wind is not significant, the behavior of the solution to equation (5) is controlled by the parameter β . For $\beta \gg 1$, the Lorentz force is insignificant to achieving force balance and hence we find that the gas pressure is a constant. For $\beta \ll 1$ we have the opposite situation where the gas pressure is insignificant. In this case the magnetic pressure and tension must balance one another. From equation (5) it is apparent that this force-free configuration occurs for $B_\phi \propto \varpi^{-1}$. Clearly this approximation cannot hold near the axis where the gas pressure (or poloidal magnetic field component) must again become important. From the z -component of Ampere’s law,

$$\frac{1}{\varpi} \frac{d\varpi B_\phi}{d\varpi} = \frac{4\pi}{c} j(\varpi) \quad (6)$$

we see that this situation describes a jet with a non-zero current density in the “core” surrounded by a current free region. The return current flows along the bow shock.

In the simulations we present in this paper, the radial force balance in the post-shock region is complicated by strong radiative cooling. In principle, since only the ambient gas is rotating and only the wind gas is magnetized, the preceding arguments should hold. We note that strong cooling in these simulations results in a mixing of the post-shock gas resulting in some rotation in the bubble plasma. The radial equilibrium of the post-shock plasma is then attained through a combination of the forces present: thermal, centrifugal, and magnetic.

Finally we note that the MHD simulations differ from their hydrodynamic counterparts in the physics occurring within the shell. Note the increased angle between the wind shock and the slip stream (the contact discontinuity) near the equator in the MHD models. The critical parameter determining the internal shell dynamics is the magnetosonic Mach number which is lower than its sonic counterpart. This implies higher pressures (magnetic + gas) within the shell. This effect was noted by Li & Shu (1996a) in their study of the interaction of a wide-angle wind with a flared accretion disk. The relative importance of the magnetic field in opening the angle between the wind shock and slip stream is increased in the presence of cooling which depletes the thermal pressure in the post shock region.

3.1. MOMENTUM DISTRIBUTION

Resolution requirements limit our studies to relatively short length and timescales compared with what is typically observed. In spite of this limitation we have attempted to characterize one simple observational characteristic of the outflows in our simulations. In a future work we provide a more complete investigation of observational consequences of larger and older simulated outflows.

In Masson & Chernin (1995) an analysis of the momentum distribution in a number of molecular outflows was presented. Averaging in slices orthogonal to the outflow axis, they found that the momentum distribution as a function of position along the outflow axis (from the base to tip of the outflow) is generally peaked in the middle of the outflow lobe. Comparing their observations to hydrodynamic models of wind blown bubbles, jet bow shocks and turbulent jet entrainment, Masson & Chernin (1995) found that none of the models could recover the momentum peak in the middle of the outflow flow.

Using a version of our code which can separately track wind and ambient material we can compare the momentum peak seen in the observations to what occurs in our models. We have repeated the calculation of the $\sigma = 0.01$, $\chi = 1$ model with this new multiple continuity equation code. In Figure 6 we plot the momentum distribution of the swept up ambient material at 4 different times. These plots shows two prominent features. One occurs near the base of the outflow and is ambient material picked up from the collapsed sheet. This peak is artificially high due to a lack of computational resolution across the slip stream. We note however that even ignoring the resolution issues, the peak at the base could never account for a significant fraction of the momentum in a mature (large scale outflow) since momentum available in a cloud core will be small compared with what has been swept up from the surrounding inter-core medium. The second and most important feature is the momentum of the outflow lobe.

At first inspection it might appear that this peak corresponds to the dense spike (jet) on the axis of the outflow. In fact, this peak does not occur at the tip of the outflow where the jet elongates the outflow lobe. Instead the momentum peak is located near the largest extent in height (z) of what would traditionally be called the “wind blown bubble”. Recall that the dense axial jet is formed from wind material. Thus it does not contribute at all to the momentum. Note also that this peak shows a clear tendency to broaden with time and coincides with the bubble evolving toward a more prolate shape. While it is a large extrapolation to extend these results to the length scales and evolutionary time scales appropriate to molecular outflow observations, the results appear suggestive in that the observed momentum distributions could be recovered if we were to let these models evolve for longer times allowing the peak to continue to broaden and smooth.

Perhaps the most promising aspect of our models is the suggestion of an observational split between a narrow jet which forms from wind material on the axis (due to axial magnetic forces) and the broader outflow formed by the rest of the wide-angle wind sweeping up ambient material. Thus the Masson & Chernin (1995) finding may point to a wide-angle wind with perhaps most of the ram pressure per unit area along the axis, but the bulk of the outward momentum at some fairly wide opening angle. By creating a jet within the wind,

the addition of magnetic fields to wide angle wind models may provide the needed physics to overcome the obstacles to finding an observationally consistent model of molecular outflows (Cabrit *et al.* 1997).

4. CONCLUSIONS

A dichotomy exists in the theoretical picture of molecular outflow formation. It appears that, to some degree, wide-angle winds were abandoned in favor of jets as the driving source for molecular outflows (Masson & Chernin 1992). Such conclusions have been, to a large extent, based upon an analysis of snowplow models (Shu *et al.* 1991) in which ambient molecular material is driven in a purely radial direction by a central, wide-angle wind. In the wake of these conclusions, it was hoped that both Herbig Haro (HH) jets and molecular outflows could be unified into a single model for outflows from YSOs. More recent studies have shown that wind-angle winds can be effective in producing molecular outflows when non-linear flow effects or appropriate wind/ambient conditions are considered (Wilkin & Stahler 1998; Delamarter *et al.* 2000; Lee *et al.* 2001). Since both HH jets and wide-angle winds are believed to be launched and collimated by magnetic fields, attempts to unify jets and molecular outflows into a single consistent phenomenon need to address the role of *magnetic forces and shocks* in shaping the flows. In this paper we have sought to address this question.

As we have shown, MHD wide-angle winds with little or no collimation at small scales give rise to a dense, jet-like, collimated outflows. We have shown that this is true even for slow magnetic rotators. Increasing either the collimation at small radii, parameterized by χ , or the magnetic field strength, parameterized by σ , toward the fast magnetic rotator limit will only enhance these results. As shown previously (Li & Shu 1996b; Matzner & McKee 1999), steady wide-angle winds with cylindrical density stratification, (consistent with MHD wind collimation), are capable of reproducing the observed characteristics of molecular outflows. In this paper we have described unsteady phenomena which result in highly collimated outflows even if there is little or no collimation to the driving wind. Extrapolating these simulations to larger radii, one can envision that as the flow evolves, an evacuated and well collimated channel is created. At larger radii, the intrinsic MHD collimation will narrow the central wind, further realizing the results of Li & Shu (1996b) and Matzner & McKee (1999). Thus we conclude that MHD wide-angle winds are capable of driving molecular outflows.

Our results are also of relevance to models of PNe and PPNe. Chevalier & Luo (1994), Różycka & Franco (1996) and García-Segura *et al.* (1999) pioneered the study of the MWBB

model in evolved, stellar outflows. As Gardiner & Frank (2001) have shown, however, even winds from slow rotators are likely to experience collimation before they are shocked via interaction with the environment. This conclusion implies that MWBB models should begin with density stratified wide-angle winds as initial conditions. The simulations presented in this paper show that when such wide-angle winds are included the resultant morphologies differ in significant ways from those obtained with spherically symmetric winds. In particular, the backflows obtained with spherical winds are suppressed when density stratified flows are included.

Future directions for this line of research include modeling both the smaller, collimation scales and larger, propagation scales. In addition, one might question the stability of such thin, dense magnetized plasma configurations seen in the axial jet. García-Segura (1997) studied the three-dimensional evolution of a magnetized wind for the case of PPNe at low resolution. That investigation found that while the dense, jet-like core does suffer some instabilities its gross morphology was not disrupted giving rise to similar outflow characteristics seen in two-dimensional cylindrically symmetric calculations (*i.e.* the formation of streamlined nose cones (Frank *et al.* 1998)). We note however, Cerqueira & de Gouveia Dal Pino (2001) study jet propagation in three-dimensional jets and contrary to two-dimensional simulations do not observe the formation of “nose-cones”.

We wish to thank Chris Matzner for helpful discussions and for providing us with information on generic wind configurations. This work was supported by NSF Grant AST-0978765, NASA Grant NAG5-8428 and the University of Rochester’s Laboratory for Laser Energetics.

REFERENCES

- Alcolea, J., Bujarrabal, V., Castro-Carrizo, A., Sanchez Contreras, C., Neri, R. & Zweigle, J. 2000, in *Asymmetrical Planetary Nebulae II: From Origins to Microstructures*, J.H. Kastner, N.Soker, & S. Rappaport eds., ASP Conf. Ser. Vol. 199, pg 347
- Balick, B. 1987, *AJ*, 94, 671
- Balick, B. 2000, in *Asymmetrical Planetary Nebulae II: From Origins to Microstructures*, J.H. Kastner, N.Soker, & S. Rappaport eds., ASP Conf. Ser. Vol. 199, pg 41
- Blackman, E. G., Frank, A. & Welch, C. 2001, *ApJ*, 546, 288
- Belcher, J. W. & MacGregor, K. B. 1976, *ApJ*, 210, 498

- Cabrit, S., Raga, A., & Gueth, F., 1997, in *Herbig-Haro Flows and the Birth of Low Mass Stars*, in IAU Symposium no. 182, eds B. Reipurth & C Bertout (Kluwer, Dordrecht), pg 163
- Cargo, P. & Gallice, G. 1997, *J. Comp. Phys.*, 136, 446
- Cantó J., Tenorio-Tagle G., & Różycka M., 1988, *A&A*, 192, 287
- Cerqueira, A. H. & de Gouveia Dal Pino, E. M. 2001, *ApJ*, 560, 779
- Chevalier, R. A. & Luo, D. 1994, *ApJ*, 421, 225
- Chernin, L. M. & Masson, C. R. 1995, *ApJ*, 455, 182
- Choudhuri, A. R. 1998, “The Physics of Fluids and Plasmas: an Introduction for Astrophysicists” (Cambridge: Cambridge Univ. Press), 359
- Delamarter, G., Frank, A. & Hartmann, L. 2000, *ApJ*, 530, 923
- Frank, A., Balick, B., Icke, V., & Mellema, G., 1993, *ApJ*, 404, L25
- Frank, A., Ryu, D., Jones, T. W. & Noriega-Crespo, A. 1998, *ApJ*, 494, L79
- Frank, A., Lery, T., Gardiner, T. A., Jones, T. W., Ryu, D. 2000, *ApJ*, 540, 342
- García-Segura, G. 1997, *ApJ*, 489, L189
- García-Segura, G., Langer, N., Różycka, M., & Franco, J. 1999, *ApJ*, 517, 767
- Gardiner, T. A. & Frank, A. 2001, *ApJ*, 557, 250
- Giuliani, J. L., Jr. 1982, *ApJ*, 256, 624
- Hartmann, L., Calvet, N. & Boss, A. 1996, *ApJ*, 464, 387
- Icke, V. 1988, *A&A*, 202, 177
- Kahn, F. D. & West, K. A. 1985, *MNRAS*, 212, 837
- Kwok, S., Purton, C., Fitzgerald, P. M., 1978, *ApJ*, 219, L125
- Lebedev, S. V., Chittenden, J. P., Beg, F. N., Bland, S. N., Ciardi, A., Ampleford, D., Hughes, S., Haines, M. G., Frank, A., Blackman, E. G. & Gardiner, T. 2002, *ApJ*, 564, 113
- Lee, C., Stone, J. M., Ostriker, E. C., & Mundy, L. G. 2001, *ApJ*, 557, 429

- Li, Z. -Y., Shu, F. H. 1996a, ApJ, 468, 261
- Li, Z. -Y., Shu, F. H. 1996b, ApJ, 472, 211
- Liu, X. -D. & Lax, P. D. 1996, J. Fluid Dynam., 5, 133
- Lax, P. D. & Liu, X. -D. 1998, SIAM J. Sci. Comp., 19, 319
- Masson, C. R. & Chernin, L. M. 1995, ApJ, 455, 182
- Masson, C. R. & Chernin, L. M. 1992, ApJ, 387, L47
- Matzner, C. D. & McKee, C. F. 1999, ApJ, 526, L109
- Mellema, G., 1997, A&A, 321, 29
- Mellema, G. & Frank, A. 1997, MNRAS, 292, 795
- Michel, F. C. 1969, ApJ, 158, 727
- “Numerical Recipes in C: The Art of Scientific Computing”, Press, W. H., Teukolsky, S. A., Vetterling, W. T. & Flannery, B. P., (Cambridge: Cambridge Univ. Press), 359
- O’Sullivan, S. & Ray, T. P. 2000, A&A, 363, 355
- Pudritz, R. E. & Konigl, A. 2000, in Protostars & Planets IV, eds. V. Mannings, A. P. Boss, and S. S. Russell (Univ. of Arizona Press), 759
- Różycka, M. & Franco, J. 1996, ApJ, 469, L127
- Reipurth B. 1997, in “Herbig-Haro Flows and the Birth of Low Mass Stars”, in IAU Symposium no. 182, eds B. Reipurth & C. Bertout (Kluwer, Dordrecht)
- Sahai R. 2000, in *Asymmetrical Planetary Nebulae II: From Origins to Microstructures*, J. H. Kastner, N. Soker, & S. Rappaport eds., ASP Conf. Ser. Vol. 199, pg 209
- Shu, F. H., Ruden, S. P., Lada, C. J., & Lizano, S. 1991, ApJ, 370, L31
- Shu, C. -W. & Osher, S. 1989, J. Comp. Phys., 83, 32
- Shu, F. H., Najita, J., Ostriker, E. C. & Shang, H. 1995, ApJ, 455, L155
- Stone, J. M. & Hardee, P. E. 2000, ApJ, 540, 192
- Wilkin, F. P. & Stahler, S. W. 1998, ApJ, 502, 661

Fig. 1.— Log(density) of purely hydrodynamic spherical wind model. ($\sigma = 0$, $\chi = 1$), $t = 65$ y. Spatial scale of grid is 600×600 AU.

Fig. 2.— Log(density) of purely hydrodynamic density stratified *wide-angle* wind model $\sigma = 0$, $\chi = 9$, $t = 36$ y.

Fig. 3.— Log(density) of magnetized spherical wind model $\sigma = 0.01$, $\chi = 1$, $t = 34$ y. Note the concave shape of the wind shock produced by the backflow from the axial jet in the post shock region.

Fig. 4.— Log(density) of magnetized density stratified *wide-angle* wind model $\sigma = 0.01$, $\chi = 9$, $t = 26$ y. Note the shape of the wind shock in now convex.

Fig. 5.— Log(density) of magnetized density stratified *wide-angle* wind model $\sigma = 0.01$, $\chi = 100$, $t = 6.5, 13, 19.5$, y. Images measure 150×600 AU.

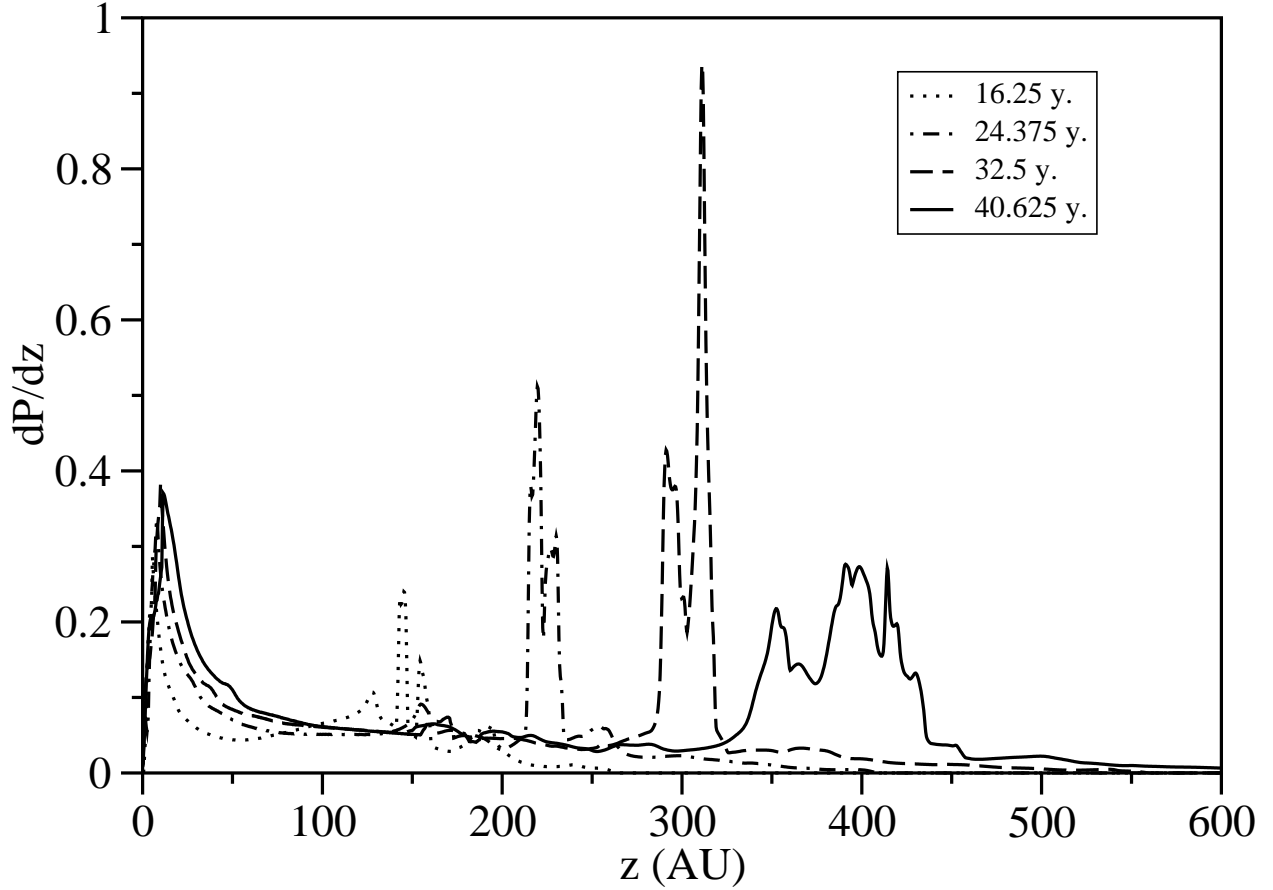


Fig. 6.— Momentum distribution in swept up ambient material as a function of position along the outflow axis for the $\sigma = 0.01$, $\chi = 1$ model at four times. Plot made by averaging in slices orthogonal to the outflow axis. The units of the momentum distribution are $M_{\odot} \text{ km s}^{-1} \text{ pc}^{-1}$. In this plot the tip of the outflow occurs at 260, 410, 560, and > 600 AU at an evolutionary time of 16, 24, 32, and 40 y respectively. Also at these times, the apex of the traditional wind blown bubble is located at 150, 225, 310, and 425 AU respectively. Thus the momentum peak at large values of z does not correspond to the tip of the outflow where the dense jet elongates the lobe but is associated swept up ambient material near the bubble apex.

This figure "f1.jpg" is available in "jpg" format from:

<http://arxiv.org/ps/astro-ph/0202243v1>

This figure "f2.jpg" is available in "jpg" format from:

<http://arxiv.org/ps/astro-ph/0202243v1>

This figure "f3.jpg" is available in "jpg" format from:

<http://arxiv.org/ps/astro-ph/0202243v1>

This figure "f4.jpg" is available in "jpg" format from:

<http://arxiv.org/ps/astro-ph/0202243v1>

This figure "f5.jpg" is available in "jpg" format from:

<http://arxiv.org/ps/astro-ph/0202243v1>